Face Encryption via Frequency-Restricted Identity-Agnostic Attacks

Xin Dong
SKLOIS, Institute of Information Engineering, CAS
School of Cyber Security, University of Chinese Academy of Sciences
Beijing, China
dongxin@iie.ac.cn

Rui Wang*
SKLOIS, Institute of Information Engineering, CAS
School of Cyber Security, University of Chinese Academy of Sciences
Beijing, China
wangrui@iie.ac.cn

Siyuan Liang
Chinese Academy of Sciences, China
Beijing, China
liangsiyuan@iie.ac.cn

Aishan Liu
NLSDE, Beihang University, China
Institute of Dataspace, Hefei, China
Beijing, China
liuaishan@buaa.edu.cn

Lihua Jing
SKLOIS, Institute of Information Engineering, CAS
School of Cyber Security, University of Chinese Academy of Sciences
Beijing, China
jinglihua@iie.ac.cn

ABSTRACT

Billions of people are sharing their daily live images on social media everyday. However, malicious collectors use deep face recognition systems to easily steal their biometric information (*e.g.*, faces) from these images. Some studies are being conducted to generate encrypted face photos using adversarial attacks by introducing imperceptible perturbations to reduce face information leakage. However, existing studies need stronger black-box scenario feasibility and more natural visual appearances, which challenge the feasibility of privacy protection. To address these problems, we propose a frequency-restricted identity-agnostic (FRIA) framework to encrypt face images from unauthorized face recognition without access to personal information. As for the weak black-box scenario feasibility, we obverse that representations of the average feature in multiple face recognition models are similar, thus we propose to utilize the average feature via the crawled dataset from the Internet as the target to guide the generation, which is also agnostic to identities of unknown face recognition systems; in nature, the low-frequency perturbations are more visually perceptible by the human vision system. Inspired by this, we restrict the perturbation in the low-frequency facial regions by discrete cosine transform to achieve the visual naturalness guarantee. Extensive experiments on several face recognition models demonstrate that our FRIA outperforms other state-of-the-art methods in generating more natural encrypted faces while attaining high black-box attack success rates of 96%. In addition, we validate the efficacy of FRIA using real-world black-box commercial API, which reveals the potential of FRIA in practice. Our codes can be found in https://github.com/XinDong10/FRIA.

CCS CONCEPTS

• **Security and privacy** → **Social network security and privacy**; **Privacy protections**; *Social aspects of security and privacy*.

KEYWORDS

privacy protection, adversarial attack, face recognition

ACM Reference Format:
Xin Dong, Rui Wang, Siyuan Liang, Aishan Liu, and Lihua Jing. 2023. Face Encryption via Frequency-Restricted Identity-Agnostic Attacks. In *Proceedings of the 31st ACM International Conference on Multimedia (MM '23), October 29–November 3, 2023, Ottawa, ON, Canada.* ACM, New York, NY, USA, 12 pages. https://doi.org/10.1145/3581783.3612233

1 INTRODUCTION

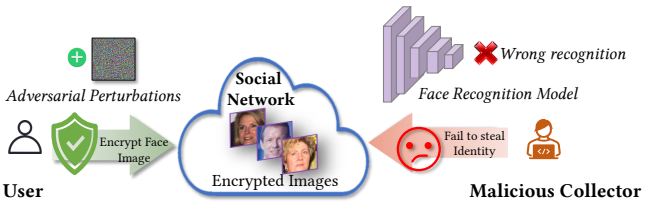

Figure 1: This paper aims to generate encrypted personal photos using adversarial attacks such that they can protect users from unauthorized face recognition systems but remain visually natural and identical to the original faces.

With the popularity of social networks, billions of people are sharing real-time images on social media every day. However, this

*Corresponding author

MM '23, October 29–November 3, 2023, Ottawa, ON, Canada.

ACM ISBN 979-8-4007-0108-5/23/10…$15.00
https://doi.org/10.1145/3581783.3612233

enormous quantity of images contains accessible, sensitive personal information (*e.g.,* faces), which can be easily stolen from photos leading to serious privacy risks [12, 21, 34, 37, 39, 42]. For example, a private company called *Clearview* collects facial data posted on social media without the user's permission. It quietly matches this facial data with facial images in the company's internal database to steal identity information [12]. So, the problem of facial privacy leakage is currently at severe risk and needs researchers give much attention to exploring and solving it.

To prevent unauthorized face recognition systems from identifying and obtaining identity information from social media, face encryption techniques have been studied to encrypt user-posted images without compromising the user-sharing experience (remaining visually natural). Traditional obfuscation-based encryption methods obscure faces with a simple mosaic [1, 33], masking [51] and blurring [36], but the visual naturalness is undesirable. Similarly, researchers adopted Generative Adversarial Networks (GANs) [14, 19, 43, 44, 52] to obfuscate faces by modifying the original facial features, which also fail to resemble the true identity and change the message that the user wants to convey. In addition, data poisoning methods [5, 39] become invalid if the system takes protection measures against the datasets. Recently, adversarial attacks [5, 46, 53, 57, 58] have been used for a benign pro-social purpose on facial privacy protection. A key guarantee of face encryption is that the facial appearance is visually discernable where the character of an adversarial attack meets this purpose. By adding visually-imperceptible perturbations that are misleading to deep neural networks (DNNs), these methods arise as possible solutions for facial image encryption.

However, current adversarial attack-based methods show two limitations: (1) *Weak black-box scenario feasibility.* Existing protection methods either assume to access the identity label of target face recognition systems or show weak attacking transferability against unknown black-box models. However, in practice, the detailed information about the target face recognition systems is unknown in advance, and attacks should be effective against these black-box models; (2) *Undesirable visual naturalness.* Existing methods fail to maintain desirable naturalness while performing satisfactory protection under black-box attacks. The added perturbations are visually-inconspicuous to humans (*e.g.,* excessive perturbations or makeups), making users reluctant to share such strange and unnatural-looking images on social media.

To solve the above-mentioned challenges, we propose a *Frequency-Restricted Identity-Agnostic (FRIA)* framework to achieve the goal of encrypting face images from unauthorized face recognition, an example is shown in Fig. 6. To improve the effectiveness of black-box attacks, we observe that various face recognition models share similar average face features. Based on that, we propose the guided feature to confuse most target face recognition systems and reduce face similarity rankings. Other than that, the guided feature is agnostic to the identities of the gallery set, which increases the practicality of the black-box attacks. To improve the naturalness of the encrypted images, we first analyze the human visual system's (HVS) sensitivity towards different frequencies. Since HVS is sensitive to the metamorphosis of smoothed regions, we restrict perturbations added in the low-frequency regions while inducing high perturbations in the high-frequency regions using the *discrete cosine transform* (DCT) so that the overall perturbations are less conspicuous to humans detection more difficult. In addition, we design an adaptive weight adjustment strategy during the optimized process to balance the encryption performance and image naturalness. Extensive experiments on multiple commonly-adopted face recognition models show that FRIA provides over 96% encryption success rate in black-box scenarios and essentially improves visual naturalness in three metrics over SOTA methods. In addition, we show the effectiveness of our method of protecting face privacy on commercial online face recognition API (Face++ [1]), which further demonstrates its potential in practice.

Our **contributions** can be summarized as follows:

- We propose a practical and effective Frequency-Restricted Identity-Agnostic (FRIA) framework to protect the privacy of facial images by generating encrypted faces using average features without identity information to improve transferability.
- To balance the attack results and naturalness of the encrypted images, we restrict low-frequency region perturbations based on DCT and use an adaptive adjustment strategy to reduce perturbation while maintaining transferability.
- Extensive comparisons on face recognition models demonstrated that FRIA is effective, with attack success rates increasing to over 96% and naturalness scores improving by 3.68 to 3.73, outperforming state-of-the-art methods. Furthermore, we achieved good results in defense experiments and online API testing.

2 RELATED WORK

2.1 Deep Face Recognition Model

In recent years, significant progress has been made in face recognition with the help of deep learning models. Face recognition aims to recognize the identity of an input face image by first detecting and aligning faces and then matching the similarity with a gallery set that stores images with known identities.

FaceNet [38] is one of the most representative models, which proposes a triplet loss function to learn discriminative features for face recognition. After that, some studies [6, 30] devoted that adopt angular softmax or additive angular margin loss to enhance the intra-class compactness and inter-class separability of features for better face recognition. MobileFace [3] proposed a lightweight face recognition model for mobile devices with SoTA performance. Other models also focus on designing appropriate loss functions to improve face recognition accuracy. For example, AM-Softmax [47] introduces additive margin softmax loss to improve the performance; CosFace [48] proposed a novel loss function for deep face recognition that incorporates a large margin cosine distance metric to improve model discrimination.

2.2 Adversarial Attacks

Adversarial examples elaborately designed perturbations that are imperceptible to humans but capable of fooling DNNs into incorrect predictions [9, 45]. A long line of work [2, 24–26, 28, 29, 32, 49] has been proposed to attack deep learning models, which can be

[1] https://www.faceplusplus.com/

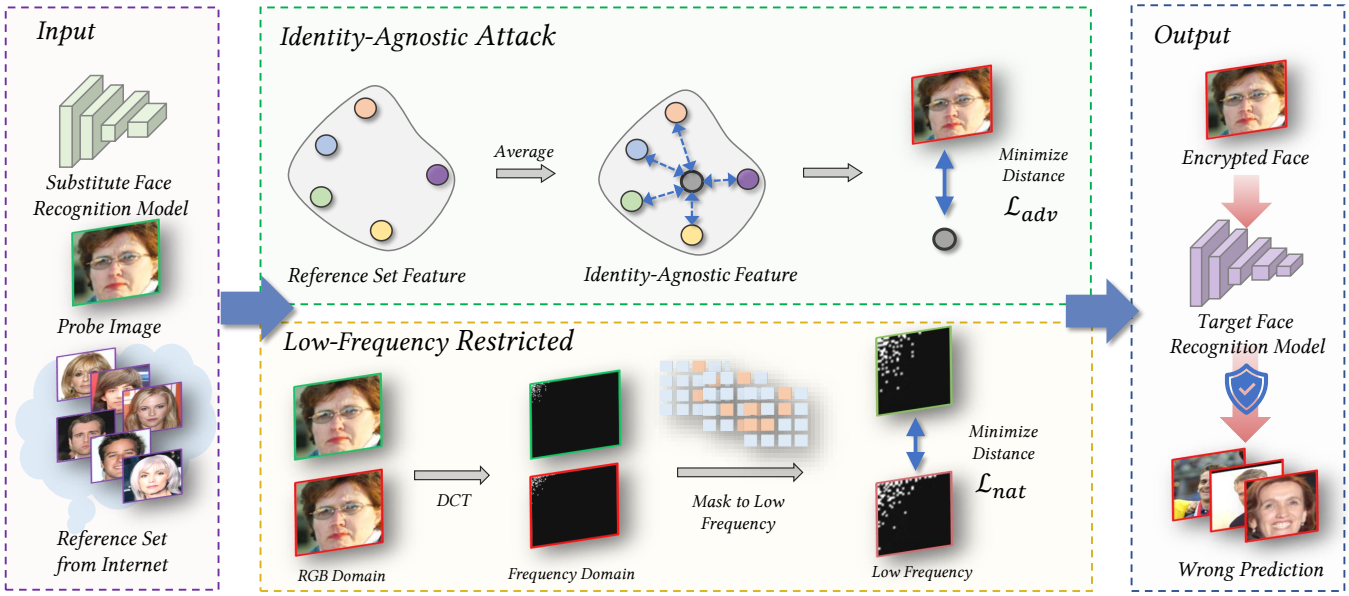

Figure 2: Illustration of our FRIA framework. Our FRIA encrypts face images from unauthorized face recognition without access to personal information.

categorized into white-box attacks [22, 50] (adversaries have direct access to the target model) and black-box attacks [20, 23] (adversaries have limited knowledge of the target model; for example, the architecture or operations may be unknown). Since the model and training datasets are not accessible, transferability is critical for black-box attacks. Attackers often employ a substitute model for adversarial examples generations and then directly perform attacks on the target victim models. Several studies devoted to improving the transferability of adversarial examples such as MIM [7], DIM [54] and TIM [8]. This paper primarily focuses on black-box attacks, *i.e.*, using adversarial attacks to protect facial privacy in the black-box setting.

2.3 Privacy Protection by Adversarial Attacks

Given that DNNs are vulnerable to adversarial examples, recent research devoted to generating adversarial attacks to protect facial privacy from being illegally learned by DNN-based face recognition systems. Lowkey [5] proposed a tool for generating adversarial samples by adding perturbations to the images of the gallery set so that the face recognition system cannot successfully steal the identity. Similarly, TIP-IM [57] proposed a targeted identity-protection iterative method to generate an adversarial identity mask that uses identity categories from the gallery set as the target for imitation attacks. Besides directly adding adversarial perturbations, some studies also investigated the possibilities of using adversarial learning from GANs. For example, AMT-GAN [14] proposed an adversarial makeup transfer GANs to make the encrypted face look more natural by replacing the user's makeup with a reference image. PP-GAN [52] proposed a de-identification adversarial sample to change the characteristics of the face with GANs.

However, these studies need stronger black-box scenario practicalities due to the access to the gallery set and weak transferable attack capabilities. Moreover, the adversarial faces they generate either add conspicuous perturbations or directly change the user's appearance, which is visually unnatural compared to the user's original image. This paper aims to generate encrypted faces using adversarial attacks and address the above problems.

3 PRELIMINARY

This section first introduces the preliminary knowledge and terminology. Next, we analyze the privacy protection challenges within the context of existing approaches.

3.1 Threat Model

In this paper, we focus on the scenario where a malicious collector uses face images from the Internet and recognizes its identity using a self-built face recognition system. Specifically, the malicious collector uses a training set D_{train} to train a feature extractor f and holds a gallery set $D_{gallery} = \{(\mathbf{x}_i^g, y_i)\}_{i=1}^N$ including N gallery face images $\mathbf{x}_i^g$ and corresponding identity label y_i.

- *Gallery set* is the set of ground-truth face images stored by the system holder, which is usually treated as similar to the verified face set (probe set) and used by the model to determine the identity information.
- *Feature extractor* is an integral component of the face recognition system. The identity inference process of a face recognition system is mostly composed of a gallery set and a feature extractor.

Specifically, the malicious collector first collects the face dataset to be verified, *i.e.*, the probe set $D_{probe} = \{(\mathbf{x}_j^p)\}$, and extracts the features of the probe image $\mathbf{x}_j^p$ using a feature extractor f. Next, the malicious attacker compares the features with those of the gallery dataset to determine the predicted identity $\hat{y}$ of the probe image

under a certain distance metric matrix $\mathcal{D}$, as follows:

$$\hat{y} = y_{\arg\min_i \mathcal{D}(f(\mathbf{x}_i^g) - f(\mathbf{x}_j^p))}. \tag{1}$$

At this time, the identity information obtained by the malicious collector through face recognition model matching is $\hat{y}$, which represents the closest identity information of the probe image, *i.e.,* the Rank-1 score. However, since the matching of faces is affected by discrepant information such as angle and illumination. Moreover, the identity information obtained from the prediction may also be a set $\hat{Y}$, *i.e.,* Rank-n score. Suppose the probe image's true identity y is in the prediction set $\hat{Y}$. In that case, there is also a possibility that the model leaks the face identity. Consequently, to maintain the identity information as much as possible, we need to make the probe image's true identity be in a lower ranking position of $\hat{Y}$.

In this paper, we focus on protecting illegal face image crawling and identity recognition, where we encrypt face images by adding adversarial attacks. Specifically, the protector should be unaware of information of the target face recognition model f, and the protector tends to generate adversarial perturbations from the substitute white-box face recognition model f_{sub} and transfer to different black-box face recognition models.

3.2 Existing Obstacles

In recent years, some works [14, 57] devoted to using adversarial examples to evade identity detection by face recognition systems while maintaining facial authenticity. However, these methods suffer from problems of *weak black-box scenario feasibility* and *poor naturalness*.

(1) *Weak black-box scenario feasibility.* TIP-IM [57] considers real-world applications to propose generating adversarial examples as encrypted faces in black-box scenarios utilizing adversarial attacks on specifically targeted identities. More specifically, TIP-IM selects a substitute face recognition model f_{sub} and encrypts the adversarial face $\mathbf{x}^a$ that is required to be close to a target image $\mathbf{x}^t$, while remaining distant from the probe face $\mathbf{x}^p$ in the model's feature space. The targeted identity y_t is extracted from the gallery set, and TIP-IM gathers face images corresponding to the identity y_t from the Internet as $\mathbf{x}^t$. The object function could be expressed as Eq. (2):

$$\begin{aligned} &\arg\min_{\mathbf{x}^a} \mathcal{D}(f_{sub}(\mathbf{x}^a) - f_{sub}(\mathbf{x}^t)) - \mathcal{D}(f_{sub}(\mathbf{x}^a) - f_{sub}(\mathbf{x}^p)), \\ &s.t. \exists y_t \in D_{gallery}, ||\mathbf{x}^a - \mathbf{x}^p||_\infty < \epsilon, \end{aligned} \tag{2}$$

where $\mathcal{D}(\cdot)$ and ∞ represent ℓ_2 distance and ℓ_∞. ϵ controls the value of adversarial perturbation.

However, the unknown gallery set and target model mainly reflect the weak black-box scenario feasibility. Firstly, in practice, identities in the gallery set are also unreachable, so the targeted attack used by current protection is infeasible. More importantly, the targeted attack aims to make the output $\hat{y}$ of the face recognition model be y_t without ensuring that the true identity y is ranked as far back in $\hat{Y}$ as possible. For example, the encryption success rate is only 70.4% when using ArcFace to attack ResNet50. Besides, the true identity y is primarily ranked in the top 5 in $\hat{Y}$. Like TIP-IM, AMT-GAN [14] also requires access to gallery set.

(2) *Poor naturalness.* The unnatural appearance of encrypted features is primarily due to the noise perturbations in the full-image region or the additional makeup. The adversarial perturbations generated by TIP and AMT-GAN encompass the entire face image. The perturbation in the cheek and forehead regions is more readily perceived by human vision due to the variation in smoothness between face regions. The encryption method that involves applying makeup to the face considers the concerns mentioned above, but it will compromise the authenticity of photo sharing by the sharers.

4 METHODOLOGY

In this section, we will describe our FRIA framework. Firstly, we illustrate the identity-agnostic method for the transferable attack improvement; we then introduce the frequency-restricted module for generating more natural appearances; finally, we describe the overall training framework. The architecture of FRIA is depicted in Fig. 7.

4.1 Identity-Agnostic Attack

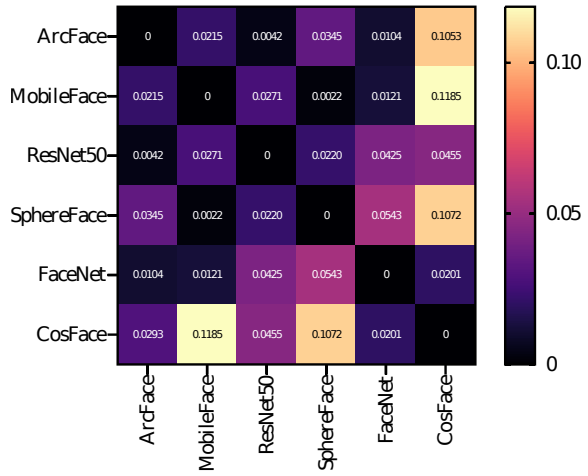

Figure 3: Similarity matrix of six face recognition models on the average feature. The lower values, the higher similarity.

Existing methods that generate encrypted faces show weak black-box attack ability (*i.e.,* impractical assumption of target identity label access and weak attack transferability). Therefore, we propose an identity-agnostic method to address the existing problems.

As demonstrated by Eq. (2), the previous method necessitates the selection of the target identity y_t from the gallery set for the targeted attack. Even though the target image $\mathbf{x}^t$ of TIP-IM is selected from the network, the identity of the target image is still selected from the gallery set. Since the malicious collector often holds the gallery set, it is practically inaccessible to the user. Based on this, we propose replacing the targeted attack with an untargeted attack, *i.e.,* identity-agnostic.

We aim to use guided features often shared between models for attacking generation to improve the attack transferability across different face recognition models. Specifically, we observe that the average values of the features for each face in a given facial dataset

share a high degree of similarity across different models. We refer to these average values as the average feature $\mathbf{R}$ and use them to guide attacking. In particular, we crawled a thousand face images of different identities from the Internet to compose a reference set $D_{ref} = \{\mathbf{x}_i^r\}_{i=1}^K$. Then we input them into the white-box substitute face recognition model f_{sub} to obtain their features set $\{f_{sub}(\mathbf{x}_i^r)\}$, and then calculate the average of the value of their features as $\mathbf{R}$ as:

$$\mathbf{R} = \frac{1}{K}\sum_{i=1}^{K} f_{sub}(\mathbf{x}_i^r), \tag{3}$$

where K is the size of D_{ref}.

To verify the above observation, we obtain the average feature set $\{\mathbf{R}_i\}$ for each of the six different substitute models (*i.e.,* ArcFace, MobileFace, ResNet50, SphereFace, FaceNet, CosFace), and then calculate the ℓ_2 distance between each other. We use $S_{i,j} = ||\mathbf{R}_i - \mathbf{R}_j||_2$ to calculate the similarity (the lower, the better similarity). As shown in Fig. 3, we can observe a high similarity between other models as the similarity matrix is close to 0. Therefore, if the encrypted image is generated by closely resembling the average feature in the feature space of the substitute model, its transferability between models can be improved since the encrypted image will also be close to the average feature of the target model. In addition, since the average feature $\mathbf{R}$ is obtained by calculating the features of a large number of different identity faces, approaching it can make the ranking of the true identity y in $\hat{Y}$ lower.

To evade the face recognition system in the feature space, we enable the encrypted face to be distant from the original face and near to $\mathbf{R}$ based on the above analysis. Inspired by the triplet state loss [38] often used in face recognition model training, we define the anchor point as encrypted face $f_{sub}(\mathbf{x}^a)$, the positive sample as average feature $\mathbf{R}$, and the negative sample as the original face image $f_{sub}(\mathbf{x}^p)$. The objective is to have the anchor sample migrate away from the negative sample and toward the positive sample. Consequently, the aim of the identity-agnostic attack is as follows:

$$\begin{aligned}\mathcal{L}_{adv} = &\arg\min_{\mathbf{x}^a} \mathcal{D}(f_{sub}(\mathbf{x}^a) - \mathbf{R})) - \mathcal{D}(f_{sub}(\mathbf{x}^a) - f_{sub}(\mathbf{x}^p)),\\ &s.t. ||\mathbf{x}^a - \mathbf{x}^p||_\infty < \epsilon.\end{aligned} \tag{4}$$

In summary, in our approach, the identity of the gallery set is irrelevant, and using average features can enhance the transferable attack capability.

4.2 Low-Frequency Restricted

Meanwhile, the added perturbations in existing techniques show weak natural appearances, which would negatively affect the user experience. In light of this, we propose a frequency-restricted method for making encrypted faces appear visually natural.

Studies have revealed that the human visual system is more sensitive to perturbation in smooth regions than in edge and texture regions [31]. Motivated by this, our method aims to restrict perturbations in flat regions for better naturalness. In particular, we aim to achieve this goal by adding the restriction in the frequency domain instead of the RGB color space. The low-frequency components depict smooth regions, and the high-frequency components represent edge and texture regions. Consequently, by limiting the perturbation of the low-frequency components, our attack could adaptive add perturbations to the face's edge areas (*e.g.,* nostrils, mouth, eyebrows), which can draw less attention to HVS.

Discrete cosine transform (DCT) [40] is a commonly used method to transform a time-domain signal into a frequency-domain signal. In our method, we define the low-frequency components of face images $\mathbf{x}_l \subset \mathbb{R}^{H\times W}$ in Eq. (5) using DCT:

$$\mathbf{x}_l = DCT(\mathbf{x}) \odot \mathbf{M}, \tag{5}$$

where $\odot$ indicates the element-wise multiplication. Here, we use a binary mask $\mathbf{M} \in \{0,1\}^{H\times W}$ to extract low-frequency information in the frequency domain. Specifically, when $i < H/10$ and $j < W/10$, the corresponding element $\mathbf{M}_{i,j}$ in the mask is set to 1, while other elements in the mask are set to 0.

To preserve naturalness, we restrict perturbation in the low-frequency region and concentrate it in the high-frequency portion of the image. Therefore, our low-frequency restriction that enhances the naturalness of an image can be illustrated by Eq. (6) as:

$$\mathcal{L}_{nat} = \arg\min_{\mathbf{x}^a} \mathcal{D}(\mathbf{x}_l^a - \mathbf{x}_l^p). \tag{6}$$

In conclusion, this approach avoids HVS's sensitivity to low-frequency changes and achieves a more realistic appearance.

4.3 Overall Training

Algorithm 1 Overall training framework of FRIA

Input: The object function $\mathcal{L}_{adv}$, $\mathcal{L}_{nat}$, a probe face $\mathbf{x}^p$, a substitute model f_{sub}, a average feature $\mathbf{R}$, the weight of object function w^{adv}, w^{nat}, the number of iteration T.

Output: The encrypted face $\mathbf{x}^a$.

```
x_0^a ← x;
for t = 1 to T do
    Get the L_total via Eq. (7);
    Compute the gradients ∇_x L_adv and ∇_x L_nat;
    Get the average magnitude Ḡ_t of the two gradients;
    Update w_t^adv and w_t^nat via Eq. (8);
    Update ∇_x L_total = ∇_x w_t^adv * L_adv + ∇_x w_t^nat * L_nat via
    Eq. (9) and generate encrypted face x^a = x_t^a via I-FGSM;
end for
return x^a.
```

Based on the above studies, our framework primarily contains two parts, *i.e.,* Identity-Agnostic Attack and Low-Frequency Restricted. The overall training objective of our FRIA framework can be illustrated as Eq. (7):

$$\begin{aligned}&\mathcal{L}_{adv} = \mathcal{D}(f_{sub}(\mathbf{x}^a) - \mathbf{R})) - \mathcal{D}(f_{sub}(\mathbf{x}^a) - f_{sub}(\mathbf{x}^p)),\\ &\mathcal{L}_{nat} = \mathcal{D}(\mathbf{x}_l^a - \mathbf{x}_l^p),\\ &\arg\min_{\mathbf{x}^a} \mathcal{L}_{total} = \mathcal{L}_{adv} + \mathcal{L}_{nat},\\ &s.t. ||\mathbf{x}^a - \mathbf{x}^p||_\infty < \epsilon.\end{aligned} \tag{7}$$

Since the objective $\mathcal{L}_{total}$ is differentiable, we can resort to iterative fast gradient descent methods (I-FGSM) [18] to minimize $\mathcal{L}_{total}$ for encrypted faces generation. However, during the optimized process, we find that the gradients' magnitudes $\mathbf{G}_t^{adv}, \mathbf{G}_t^{nat}$ of $\mathcal{L}_{adv}$ and $\mathcal{L}_{nat}$ w.r.t $\mathbf{x}$ differ significantly. Inspired by GradNorm [4]

that can handle imbalances between multiple tasks, we propose an adaptive adjustment strategy to balance $\mathbf{G}_t^{adv}$ and $\mathbf{G}_t^{nat}$.

In particular, during each iteration, we calculate the average magnitude $\overline{\mathbf{G}}$ of the two gradient terms. Next, by adjusting the weights w^{adv}, w^{nat} of the two loss terms $\mathcal{L}_{adv}$ and $\mathcal{L}_{nat}$, we can bring the two gradients close to $\overline{\mathbf{G}}$. We first calculate the absolute value of the difference between the two gradients' magnitudes relative to the average magnitude at the t-th iteration and then update w^{adv}, w^{nat} in the t-th iteration as Eq. (8) shows:

$$w_t^{adv} = 10^{\mathbf{G}_t^{adv} - \overline{\mathbf{G}}_t}, w_t^{nat} = 10^{\mathbf{G}_t^{nat} - \overline{\mathbf{G}}_t}, \tag{8}$$

where w_t^{adv} and w_t^{nat} are updated weights used in t-th iteration. The L_{total} is eventually expressed in t-th iteration as Eq. (9):

$$\mathcal{L}_{total} = w_t^{adv} * \mathcal{L}_{adv} + w_t^{nat} * \mathcal{L}_{nat}. \tag{9}$$

In summary, to achieve the unawareness of the gallery set and improve transferable attack capability, FRIA uses untargeted attack and average feature via $\mathcal{L}_{adv}$ in Eq. (7). To make the encrypted face more natural, FRIA adds the perturbation to high frequencies from the frequency domain perspective via $\mathcal{L}_{nat}$ in Eq. (7). Ultimately, FRIA continuously updates the weights to balance the magnitudes of the gradients in Eq. (9) to relieve the conflict between the two tasks. The overall pseudo-algorithm can be found in Alg. 1.

5 EXPERIMENTS

In this section, we first describe the experimental setup on black-box attack, then analyze our FRIA for transferable attack capability and naturalness, and finally provide online API testing, and performance on defense methods.

5.1 Experimental Settings

This section describes our experimental settings on the datasets, target models, implementation details, and evaluation metrics.

Datasets. Following [57], we select a gallery set and a probe set from LFW [15], and MegFace [17] datasets. Specifically, we selected 500 face images of different identities as D_{probe}, and other images of these identities composed part of the $D_{gallery}$. Then, we selected another 500 identities to compose the other part of $D_{gallery}$. For D_{ref}, we randomly selected 1000 face images from the Celeb-A dataset [16].

Target Models. Following [59], we select ArcFace, MobileFace, ResNet50, CosFace, ShperFace, and FaceNet as the target face recognition models with different architectures and loss functions and one commercial face recognition API, *i.e.,* Face++ [1].

Compared Methods. We compare the transferable attack capability of encrypted faces generated by our frequency-restricted identity-agnostic framework and other adversarial attack methods, including DIM [54] that enhances the transferable capability by diversifying the input samples in image classification. In addition, we compare two of the state-of-the-art methods proposed for generating encrypting faces by adversarial examples, *i.e.,* TIP-IM [57] and AMT-GAN [14].

For fairness, we set the number of iterations to 50, the learning rate to 1.5, and the perturbation size to 12 under the constraint of ℓ_∞ for DIM and ours FAIR. Our experiments were conducted on NVIDIA 3090 GPU with 24GB of memory.

Evaluation Metrics. To evaluate the performance of transferable attack capability, we define encrypted success rank-1 (ESR-1) and encrypted success rank-5 (ESR-5).

Specifically, if the output $\hat{y}$ of an encrypted face for the malicious collector is not equal to the true identity y of the probe image, then its ESR-1 value is 1, otherwise 0. Similarly, if y is not at the top five of $\hat{Y}$, ESR-5 is also the same. Therefore, *the higher the value, the stronger the transferable attack capability.*

To measure the naturalness of encrypted images, we used the PSNR (dB) [13] and SSIM [10], which are commonly used in previous works. Similarly, *the higher value of PSNR and SSIM, the more natural the encrypted face is.* We also conduct human perception studies on one of the most commonly used crowdsourcing platforms. Especially participants were asked to choose an encrypted face that looks most natural, generated by DIM, AMT-GAN, TIP-IM, and our FAIR. Then we counted the number of choices for each of the four methods as response scores separately. Responses scores were collected from 100 anonymous Amazon Mechanical Turk (AMT) participants.

5.2 Results for Black-box Protection

In this section, we compare our frequency-restricted identity-agnostic framework (FRIA) and other SoTA methods of encrypted faces to prove the improvement of the transferability in multiple face recognition models.

In Tab. 1, we first compute the ESR-1 and ESR-5 of the recognition model on the unencrypted probe image to represent the recognition, that is 'ORIGINAL'. ↑ means that the larger the value, the higher the encrypt success rate. We also investigated the impact of employing GAN to generate adversarial perturbations encrypted faces, that is 'AMT-GAN'. Specifically, we use the pretrained AMT-GAN [14] model to generate encrypted features on 500 probe images and to calculate ESR-1 and ESR-5 for untargeted attacks. Since this paper focuses on the attack capability of encrypted faces during an untargeted attack, we set the objective function $\arg\min_{\mathbf{x}^a} \mathcal{L}_{DIM} = -\mathcal{D}(f_{sub}(\mathbf{x}^a) - f_{sub}(\mathbf{x}^p))$ in DIM to the untargeted attack form, *i.e.,* 'DIM', to generate encrypted faces. In addition, to fairly compare the TIP-IM methods, we utilize the results of the untargeted attack described in their papers with Rank-1-UT and Rank-5-UT, *i.e.,* 'TIP-IM'. We evaluate the effectiveness of transfer-based attacks on FRIA and the above methods in three white-box face recognition models and six black-box face recognition models.

We choose Arcface, MobileFace, and ResNet50 as substitute models to generate encrypted faces. Analyzing Tab. 1 enables us to draw multiple inferences: (1) Due to the use of the average feature, the performance of our FRIA is nearly twice as excellent as that of our DIM, which also employs untargeted attacks. However, TIP-IM utilizes a targeted attack because the objective is more complex than an untargeted attack, and its performance is inferior to that of FRIA. In general, our proposed FRIA's transferable attack is **superior to SOTA methods**. (2) FRIA outperforms the previous best method by 3.0% to 11.4% in ESR-1 and by 3.6% to 26.0% in ESR-5 and obtains over 95% attack success rate on the majority of face recognition models in black-box scenarios. This result demonstrates that encrypted faces by FRIA have **superior attack transferability** on the majority of threat models; (3) Evidently, the enhancement of

Table 1: Encrypt success rank-1 (ESR-1) and rank-5 (ESR-5) (%) of black-box. The best results are marked in bold.

	Method	ArcFace [6]		MobileFace [3]		ResNet50[11]		SphereFace [30]		FaceNet [38]		CosFace [48]	
		ESR-1↑	ESR-5↑	ESR-1↑	ESR-5↑	ESR-1↑	ESR-5↑	ESR-1↑	ESR-5↑	ESR-1↑	ESR-5↑	ESR-1↑	ESR-5↑
	ORIGINAL	1.0	0.6	1.6	0.8	2.6	1.4	24.8	19.8	16.0	8.8	12.4	8.4
	AMT-GAN [14]	8.2	17.2	32.2	53.8	24.8	42.4	94.8	93.8	96.6	93.8	96.6	94.4
ArcFace	DIM [54]	100	100	96.4	93.0	91.8	80.6	87.0	84.4	80.6	74.0	87.2	83.4
	TIP-IM [57]	97.4	96.4	79.4	68.8	70.4	56.8	85.2	76.6	73.4	63.4	84.0	73.8
	FRIA	**100**	**100**	**96.6**	**94.2**	**92.0**	**82.0**	**100**	**98.2**	**89.8**	**88.6**	**87.4**	**84.0**
MobileFace	DIM [54]	65.2	50.8	97.0	94.2	80.8	68.2	99.4	98.0	99.8	99.6	99.8	99.8
	TIP-IM [57]	68.6	58.8	96.6	94.8	81.4	71.2	84.4	74.0	77.6	60.4	79.4	68.2
	FRIA	**80.4**	**70.6**	**100**	**100**	**97.8**	**96.0**	**100**	**98.8**	**100**	**99.6**	**99.8**	**99.8**
ResNet50	DIM [54]	63.2	48.0	80.0	68.2	97.8	94.2	**100**	**98.8**	99.6	98.8	99.8	99.6
	TIP-IM [57]	**83.6**	59.6	87.0	81.8	96.8	94.6	85.8	75.0	79.4	65.4	83.6	73.0
	FRIA	81.8	**70.6**	**95.8**	**94.6**	**100**	**100**	99.6	98.4	**99.8**	**99.4**	**99.8**	**99.8**

FRIA on ESR-5 is more significant than that on ESR-1 relative to other models. For instance, when ResNet50 was used as a substitute model to attack MobileFace, ESR-5 and ESR-1 increased by 12.9 and 8.8 percent, respectively. In addition, ESR-5 at FRIA is similar to ESR-1, only decreasing from 1.2% to 11.2%. This **confirms our hypothesis** that an average feature can bring the encrypted face close to the majority of fictitious identities, enabling the true identity to be concealed effectively from an unidentified third-party face recognition system; (4) It can be seen that most methods significantly have better attack results than the last three recognition methods because the recognition performance of these models is not well. For example, the encryption success rate of AMT-GAN on the first three target models is less than 54%, but on the last three target models is above 93%.

5.3 Visual Naturalness Evaluation

In this section, we compare the naturalness of the generated encrypted faces with other methods. The naturalness of the generated encrypted features using ArcFace will be evaluated from both qualitative and quantitative angles. We use three evaluation indicators for qualitative evaluation. To calculate PSNR(dB) [13] and SSIM [10], we use encrypted faces with their corresponding probe images. In addition, we obtain response scores from 100 anonymous Amazon Mechanical Turk (AMT) participants, *i.e.,* let participants select the encrypted face that appears most natural in comparison to the unencrypted probing image, and we set the response score of the 'ORIGINAL' to 100. ↑ means that the larger the value, the higher the naturalness.

As shown in Tab. 2, AMT-GAN has a very low PSNR of 19.50 because it makes a significant change in the makeup style of the whole face, but it has a good SSIM performance of 0.7873 and response score of 33, because it does not change the structure information too much. For DIM, although its PSNR of 28.18 is not much different from FRIA, its relatively low SSIM and response score indicates that it corrupts more structural information of probe images. TIP-IM has the lowest values in all metrics, which may be caused by using MIM [7]. Our method outperforms in three metrics, *i.e.,* PSNR, SSIM, and response score improve to 28.99, 0.7964, 64.

In addition, to quantitatively evaluate the image quality of the generated encrypted faces, we present encrypted faces generated by AMT-GAN, DIM, TIP-IM, and our FRIA in Fig. 4. Although AMT-GAN does not produce significant perturbations to the image, the visage after the makeup application differs from the probe image. It generates twisted distortion, making it look unreal. TIP-IM has the most significant perturbations. Even though DIM has fewer perturbations than TIP-IM, the noise is still quite large, rendering the encrypted visage unnatural. Our modifications to the original probe image are minimal and primarily concentrated on the face's edges and texture. This result means that our proposed low-frequency restriction allows the addition of disturbance to the high-frequency region of the image and increases the naturalness of the image.

Table 2: Evaluation of Naturalness. Our FRIA performs best in all naturalness metrics.

	Method	PSNR↑	SSIM↑	RESPONSE↑
	ORIGINAL	∞	1.0	100
	AMT-GAN [14]	19.50	0.7873	29
ArcFace	DIM [54]	28.18	0.7769	7
	TIP-IM [57]	25.26	0.7567	2
	FRIA	**28.99**	**0.7964**	**62**

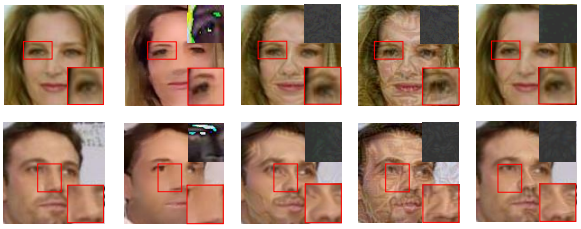

Figure 4: Visualization of encrypted faces generated by different methods, we zoomed in on the regions where the perturbations were added.

5.4 Studies of Online Face Recognition API in the Real-world

In this section, we compare the effectiveness of FRIA with other SoTA methods for attacks on commercial API Face++ face recognition systems [1]. Face++ is an open-source and free API that allows users to compare two images of faces.

We calculate the average similarity (AS) between 500 encrypted features generated by ArcFace and their corresponding probe images provided by Face++ to indicate attack capability. The value of the metric decreases, and the attack capability increases. In addition, to test the ability of encrypted faces to conceal their true identities and consider the online API's limited resources, we selected 20 probe images. We input them into Face++ with the gallery set and calculated their true identities' average ranking position (AP).

As shown in Fig. 5, our method compared AS to AMT-GAN, DIM, and TIP-IM decreased by 6.84, 3.87, and 3.29. Thus encrypted faces generated by FRIA can significantly reduce the similarity to the true identity. Our FRIA reached 39.00 on AP, significantly higher than the other indicators, which only reached a maximum of 5.30, as shown in Fig. 5. In summary, the reduction in the average similarity metric indicates that the encrypted face generated by FRIA can successfully confuse commercial API Face++. The increase in the average ranking position suggests that FRIA can enhance the concealment of true identities.

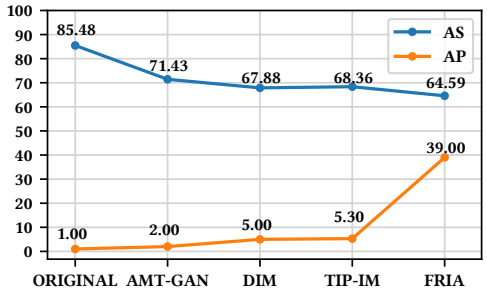

Figure 5: Results of our FRIA and other compared methods on black-box commercial FR API Face++. Our FRIA performs best under AS and AP metrics on Face++.

5.5 Black-box Attack Against Defense Methods

Table 3: performance of encrypted faces on defense methods.

Method	BitRed [56]		JPEG (75) [41]		NRP [35]	
	ESR-1↑	ESR-5↑	ESR-1↑	ESR-5↑	ESR-1↑	ESR-5↑
ORIGINAL	6.4	4.0	2.8	1.6	**90.6**	**83.6**
AMT-GAN [14]	45.8	65.2	33.8	53.4	43.4	63.8
TIP-IM [57]	47.6	24.0	71.2	42.8	18.4	11.4
FRIA	**91.2**	**83.4**	**96.2**	**93.4**	29.4	44.8

Some existing models [27, 55, 60] include defense mechanisms against adversarial attacks. In this subsection, we assess the attack capability of encrypted faces generated by FRIA and other methods using ArcFace as a substitute model to attack MobileFace against some commonly used defense methods.

We use existing pre-processing defense methods that work to remove the adversarial of the generated adversarial examples. BitRed [56] proposes a feature squeezing method that reduces the color bit depth of each pixel to detect adversarial examples; JPEG compression [41] compress adversarial perturbations with QF = 75; NRP [35] proposes a neural representation purifier to clean adversarially perturbed images. We primarily use these defense methods to pre-process encrypted face images before inputting them into the face recognition model to assess the attack capability of ESR-1 and ESR-5.

As demonstrated in Tab. 3, we first test ESR-1 and ESR-5 of the original probe image when confronting 'ORIGINAL' defense methods. ↑ means that the larger the value, the higher the encrypt success rate. It is reasonable to expect that the encryption success rank of the original probe image on the target model would remain very low after being processed by the defense method. Still, the encryption success rate increases significantly to over 90 percent after processing them by NRP due to its purification effect on the image, which drastically removes facial features. Therefore, although the NRP method works as a method of defense, it has an enormous negative impact on the accuracy of face recognition models. For AMT-GAN, it performs better than TIP-IM and FRIA only in NRP, which removed facial features like the original probe images. On BitRed and JPEG, ESR-1 and ESR-5 of 'ORIGINAL' is at most 6.4%, indicating that they do not affect face recognition models' accuracy. Our FRIA performs better than the best TIP-IM by at most 59.4 and 50.6, respectively, so that encrypted faces generated by FRIA do not lose adversarial easily.

6 CONCLUSION

This paper proposes the FRIA framework to encrypt face images with frequency-restricted and identity-agnostic attacks to address the face privacy leakage problem. Extensive experiments on multiple face recognition datasets using diverse models demonstrate that our FRIA outperforms others in generating more natural encrypted faces while attaining high black-box attack success rates. Experiments on real-world black-box commercial API further reveal the potential of our FRIA in practice.

In the future, we would like to design strategies that could adaptively learn the perturbation magnitudes added at specific frequency domains. Additionally, we are interested in investigating the possibilities of implementing our FRIA as a pre-processing tool for social media websites.

ACKNOWLEDGMENTS

This work was supported in part by the National Natural Science Foundation of China Under Grants No.62206009, No.62176253, and No.U20B2066.

REFERENCES

[1] Amine Boulemtafes, Abdelouahid Derhab, and Yacine Challal. 2020. A review of privacy-preserving techniques for deep learning. *Neurocomputing* 384 (2020), 21–45.

[2] Nicholas Carlini and David Wagner. 2017. Towards evaluating the robustness of neural networks. In *2017 ieee symposium on security and privacy (sp)*. Ieee, 39–57.

[3] Sheng Chen, Yang Liu, Xiang Gao, and Zhen Han. 2018. Mobilefacenets: Efficient cnns for accurate real-time face verification on mobile devices. In *Biometric Recognition: 13th Chinese Conference, CCBR 2018, Urumqi, China, August 11-12, 2018, Proceedings 13*. Springer, 428–438.

[4] Zhao Chen, Vijay Badrinarayanan, Chen-Yu Lee, and Andrew Rabinovich. 2018. Gradnorm: Gradient normalization for adaptive loss balancing in deep multitask networks. In *International conference on machine learning*. PMLR, 794–803.

[5] Valeriia Cherepanova, Micah Goldblum, Harrison Foley, Shiyuan Duan, John Dickerson, Gavin Taylor, and Tom Goldstein. 2021. Lowkey: Leveraging adversarial attacks to protect social media users from facial recognition. *arXiv preprint arXiv:2101.07922* (2021).

[6] Jiankang Deng, Jia Guo, Niannan Xue, and Stefanos Zafeiriou. 2019. Arcface: Additive angular margin loss for deep face recognition. In *Proceedings of the IEEE/CVF conference on computer vision and pattern recognition*. 4690–4699.

[7] Yinpeng Dong, Fangzhou Liao, Tianyu Pang, Hang Su, Jun Zhu, Xiaolin Hu, and Jianguo Li. 2018. Boosting adversarial attacks with momentum. In *Proceedings of the IEEE conference on computer vision and pattern recognition*. 9185–9193.

[8] Yinpeng Dong, Tianyu Pang, Hang Su, and Jun Zhu. 2019. Evading defenses to transferable adversarial examples by translation-invariant attacks. In *Proceedings of the IEEE/CVF Conference on Computer Vision and Pattern Recognition*. 4312–4321.

[9] Ian J Goodfellow, Jonathon Shlens, and Christian Szegedy. 2014. Explaining and harnessing adversarial examples. *arXiv preprint arXiv:1412.6572* (2014).

[10] Muhammad Zaid Hameed and Andras Gyorgy. 2021. Perceptually constrained adversarial attacks. *arXiv preprint arXiv:2102.07140* (2021).

[11] Kaiming He, Xiangyu Zhang, Shaoqing Ren, and Jian Sun. 2016. Identity mappings in deep residual networks. In *Computer Vision–ECCV 2016: 14th European Conference, Amsterdam, The Netherlands, October 11–14, 2016, Proceedings, Part IV 14*. Springer, 630–645.

[12] Kashmir Hill and Aaron Krolik. 2019. How photos of your kids are powering surveillance technology. *The New York Times* 11 (2019).

[13] Alain Hore and Djemel Ziou. 2010. Image quality metrics: PSNR vs. SSIM. In *2010 20th international conference on pattern recognition*. IEEE, 2366–2369.

[14] Shengshan Hu, Xiaogeng Liu, Yechao Zhang, Minghui Li, Leo Yu Zhang, Hai Jin, and Libing Wu. 2022. Protecting facial privacy: generating adversarial identity masks via style-robust makeup transfer. In *Proceedings of the IEEE/CVF Conference on Computer Vision and Pattern Recognition*. 15014–15023.

[15] Gary B Huang, Marwan Mattar, Tamara Berg, and Eric Learned-Miller. 2008. Labeled faces in the wild: A database forstudying face recognition in unconstrained environments. In *Workshop on faces in'Real-Life'Images: detection, alignment, and recognition*.

[16] Tero Karras, Timo Aila, Samuli Laine, and Jaakko Lehtinen. 2017. Progressive growing of gans for improved quality, stability, and variation. *arXiv preprint arXiv:1710.10196* (2017).

[17] Ira Kemelmacher-Shlizerman, Steven M Seitz, Daniel Miller, and Evan Brossard. 2016. The megaface benchmark: 1 million faces for recognition at scale. In *Proceedings of the IEEE conference on computer vision and pattern recognition*. 4873–4882.

[18] Alexey Kurakin, Ian Goodfellow, and Samy Bengio. 2016. Adversarial machine learning at scale. *arXiv preprint arXiv:1611.01236* (2016).

[19] Tao Li and Lei Lin. 2019. Anonymousnet: Natural face de-identification with measurable privacy. In *Proceedings of the IEEE/CVF conference on computer vision and pattern recognition workshops*. 0–0.

[20] Siyuan Liang, Longkang Li, Yanbo Fan, Xiaojun Jia, Jingzhi Li, Baoyuan Wu, and Xiaochun Cao. 2022. A Large-Scale Multiple-objective Method for Black-box Attack Against Object Detection. In *Computer Vision–ECCV 2022: 17th European Conference, Tel Aviv, Israel, October 23–27, 2022, Proceedings, Part IV*. Springer, 619–636.

[21] Siyuan Liang, Aishan Liu, Jiawei Liang, Longkang Li, Yang Bai, and Xiaochun Cao. 2022. Imitated Detectors: Stealing Knowledge of Black-box Object Detectors. In *Proceedings of the 30th ACM International Conference on Multimedia*. 4839–4847.

[22] Siyuan Liang, Xingxing Wei, Siyuan Yao, and Xiaochun Cao. 2020. Efficient adversarial attacks for visual object tracking. In *Computer Vision–ECCV 2020: 16th European Conference, Glasgow, UK, August 23–28, 2020, Proceedings, Part XXVI 16*. Springer, 34–50.

[23] Siyuan Liang, Baoyuan Wu, Yanbo Fan, Xingxing Wei, and Xiaochun Cao. 2022. Parallel rectangle flip attack: A query-based black-box attack against object detection. *arXiv preprint arXiv:2201.08970* (2022).

[24] Aishan Liu, Jun Guo, Jiakai Wang, Siyuan Liang, Renshuai Tao, Wenbo Zhou, Cong Liu, Xianglong Liu, and Dacheng Tao. 2023. X-Adv: Physical Adversarial Object Attacks against X-ray Prohibited Item Detection. *ArXiv* (2023).

[25] Aishan Liu, Tairan Huang, Xianglong Liu, Yitao Xu, Yuqing Ma, Xinyun Chen, Stephen J Maybank, and Dacheng Tao. 2020. Spatiotemporal attacks for embodied agents. In *ECCV*.

[26] Aishan Liu, Xianglong Liu, Jiaxin Fan, Yuqing Ma, Anlan Zhang, Huiyuan Xie, and Dacheng Tao. 2019. Perceptual-sensitive gan for generating adversarial patches. In *AAAI*.

[27] Aishan Liu, Xianglong Liu, Hang Yu, Chongzhi Zhang, Qiang Liu, and Dacheng Tao. 2021. Training robust deep neural networks via adversarial noise propagation. *TIP* (2021).

[28] Aishan Liu, Jiakai Wang, Xianglong Liu, Bowen Cao, Chongzhi Zhang, and Hang Yu. 2020. Bias-based universal adversarial patch attack for automatic check-out. In *ECCV*.

[29] Shunchang Liu, Jiakai Wang, Aishan Liu, Yingwei Li, Yijie Gao, Xianglong Liu, and Dacheng Tao. 2022. Harnessing Perceptual Adversarial Patches for Crowd Counting. In *ACM CCS*.

[30] Weiyang Liu, Yandong Wen, Zhiding Yu, Ming Li, Bhiksha Raj, and Le Song. 2017. Sphereface: Deep hypersphere embedding for face recognition. In *Proceedings of the IEEE conference on computer vision and pattern recognition*. 212–220.

[31] Cheng Luo, Qinliang Lin, Weicheng Xie, Bizhu Wu, Jinheng Xie, and Linlin Shen. 2022. Frequency-driven imperceptible adversarial attack on semantic similarity. In *Proceedings of the IEEE/CVF Conference on Computer Vision and Pattern Recognition*. 15315–15324.

[32] Aleksander Madry, Aleksandar Makelov, Ludwig Schmidt, Dimitris Tsipras, and Adrian Vladu. 2017. Towards deep learning models resistant to adversarial attacks. *arXiv preprint arXiv:1706.06083* (2017).

[33] Richard McPherson, Reza Shokri, and Vitaly Shmatikov. 2016. Defeating image obfuscation with deep learning. *arXiv preprint arXiv:1609.00408* (2016).

[34] Paul Mozur. 2018. Inside China's dystopian dreams: AI, shame and lots of cameras. *The New York Times* 8 (2018), 1.

[35] Muzammal Naseer, Salman Khan, Munawar Hayat, Fahad Shahbaz Khan, and Fatih Porikli. 2020. A self-supervised approach for adversarial robustness. In *Proceedings of the IEEE/CVF Conference on Computer Vision and Pattern Recognition*. 262–271.

[36] Seong Joon Oh, Rodrigo Benenson, Mario Fritz, and Bernt Schiele. 2016. Faceless person recognition: Privacy implications in social media. In *Computer Vision–ECCV 2016: 14th European Conference, Amsterdam, The Netherlands, October 11-14, 2016, Proceedings, Part III 14*. Springer, 19–35.

[37] ADAM SATARIANO. 2019. Police use of facial recognition is accepted by British court. *The New York Times* 4 (2019).

[38] Florian Schroff, Dmitry Kalenichenko, and James Philbin. 2015. Facenet: A unified embedding for face recognition and clustering. In *Proceedings of the IEEE conference on computer vision and pattern recognition*. 815–823.

[39] Shawn Shan, Emily Wenger, Jiayun Zhang, Huiying Li, Haitao Zheng, and Ben Y Zhao. 2020. Fawkes: Protecting privacy against unauthorized deep learning models. In *Proceedings of the 29th USENIX Security Symposium*.

[40] Yash Sharma, Gavin Weiguang Ding, and Marcus Brubaker. 2019. On the effectiveness of low frequency perturbations. *arXiv preprint arXiv:1903.00073* (2019).

[41] Richard Shin and Dawn Song. 2017. Jpeg-resistant adversarial images. In *NIPS 2017 Workshop on Machine Learning and Computer Security*, Vol. 1. 8.

[42] Dechao Sun, Hong Huang, Dongsong Zheng, Haoliang Hu, Chunyue Bi, and Renfang Wang. 2022. Face security authentication system based on deep learning and homomorphic encryption. *Security and Communication Networks* 2022 (2022).

[43] Qianru Sun, Liqian Ma, Seong Joon Oh, Luc Van Gool, Bernt Schiele, and Mario Fritz. 2018. Natural and effective obfuscation by head inpainting. In *Proceedings of the IEEE Conference on Computer Vision and Pattern Recognition*. 5050–5059.

[44] Qianru Sun, Ayush Tewari, Weipeng Xu, Mario Fritz, Christian Theobalt, and Bernt Schiele. 2018. A hybrid model for identity obfuscation by face replacement. In *Proceedings of the European conference on computer vision (ECCV)*. 553–569.

[45] Christian Szegedy, Wojciech Zaremba, Ilya Sutskever, Joan Bruna, Dumitru Erhan, Ian Goodfellow, and Rob Fergus. 2013. Intriguing properties of neural networks. *arXiv preprint arXiv:1312.6199* (2013).

[46] Simen Thys, Wiebe Van Ranst, and Toon Goedemé. 2019. Fooling automated surveillance cameras: adversarial patches to attack person detection. In *Proceedings of the IEEE/CVF conference on computer vision and pattern recognition workshops*. 0–0.

[47] Feng Wang, Jian Cheng, Weiyang Liu, and Haijun Liu. 2018. Additive margin softmax for face verification. *IEEE Signal Processing Letters* 25, 7 (2018), 926–930.

[48] Hao Wang, Yitong Wang, Zheng Zhou, Xing Ji, Dihong Gong, Jingchao Zhou, Zhifeng Li, and Wei Liu. 2018. Cosface: Large margin cosine loss for deep face recognition. In *Proceedings of the IEEE conference on computer vision and pattern recognition*. 5265–5274.

[49] Jiakai Wang, Aishan Liu, Zixin Yin, Shunchang Liu, Shiyu Tang, and Xianglong Liu. 2021. Dual attention suppression attack: Generate adversarial camouflage in physical world. In *CVPR*.

[50] Xingxing Wei, Siyuan Liang, Ning Chen, and Xiaochun Cao. 2018. Transferable adversarial attacks for image and video object detection. *arXiv preprint arXiv:1811.12641* (2018).

[51] Michael J Wilber, Vitaly Shmatikov, and Serge Belongie. 2016. In *2016 IEEE Winter Conference on Applications of Computer Vision (WACV)*. IEEE, 1–9.

[52] Yifan Wu, Fan Yang, and Haibin Ling. 2018. Privacy-protective-gan for face de-identification. *arXiv preprint arXiv:1806.08906* (2018).

[53] Zuxuan Wu, Ser-Nam Lim, Larry S Davis, and Tom Goldstein. 2020. Making an invisibility cloak: Real world adversarial attacks on object detectors. In *Computer Vision–ECCV 2020: 16th European Conference, Glasgow, UK, August 23–28, 2020,*

Proceedings, Part IV 16. Springer, 1–17.
[54] Cihang Xie, Zhishuai Zhang, Yuyin Zhou, Song Bai, Jianyu Wang, Zhou Ren, and Alan L. Yuille. 2019. Improving Transferability of Adversarial Examples With Input Diversity. In *Proceedings of the IEEE/CVF Conference on Computer Vision and Pattern Recognition (CVPR)*.
[55] Han Xu, Yao Ma, Hao-Chen Liu, Debayan Deb, Hui Liu, Ji-Liang Tang, and Anil K Jain. 2020. Adversarial attacks and defenses in images, graphs and text: A review. *International Journal of Automation and Computing* 17 (2020), 151–178.
[56] Weilin Xu, David Evans, and Yanjun Qi. 2017. Feature squeezing: Detecting adversarial examples in deep neural networks. *arXiv preprint arXiv:1704.01155* (2017).
[57] Xiao Yang, Yinpeng Dong, Tianyu Pang, Hang Su, Jun Zhu, Yuefeng Chen, and Hui Xue. 2021. Towards face encryption by generating adversarial identity masks. In *Proceedings of the IEEE/CVF International Conference on Computer Vision*. 3897–3907.
[58] Xiao Yang, Chang Liu, Longlong Xu, Yikai Wang, Yinpeng Dong, Ning Chen, Hang Su, and Jun Zhu. 2023. Towards Effective Adversarial Textured 3D Meshes on Physical Face Recognition. *arXiv preprint arXiv:2303.15818* (2023).
[59] Xiao Yang, Dingcheng Yang, Yinpeng Dong, Hang Su, Wenjian Yu, and Jun Zhu. 2020. Robfr: benchmarking adversarial robustness on face recognition. *arXiv preprint arXiv:2007.04118* (2020).
[60] Chongzhi Zhang, Aishan Liu, Xianglong Liu, Yitao Xu, Hang Yu, Yuqing Ma, and Tianlin Li. 2021. Interpreting and Improving Adversarial Robustness of Deep Neural Networks with Neuron Sensitivity. *IEEE Transactions on Image Processing* (2021).

A DETAILED INFORMATION ON TARGET MODELS

In this subsection, we specify information about the target models in Tab. 4, including backbones and loss functions.

Table 4: Detailed information of target models.

Model	Backbone	Loss
FaceNet	InceptionResNetV1	Triplet loss
SphereFace	Sphere20	A-softmax
CosFace	Sphere20	LMCL
MobileFace	MobileFaceNet	LMCL
ResNet50	ResNet50	LMCL
ArcFace	IR-SE50	ArcFace

B VISUAL NATURALNESS EVALUATION

In this section, we complement the experiments evaluating the naturalness of generated encrypted images in Section 5.3 of the main text by comparing encrypted faces generated by MobileFace and ResNet50 under each method. Since RESPONSE requires separate models for statistics, the results of the two models are shown in Tab. 5 and Tab. 6, respectively. Obviously, with MobileFace and ResNet50, the encrypted faces generated by our FRIA achieve the best in all three naturalness evaluation metrics.

Table 5: Evaluation of Naturalness on MobileFace. Our FRIA performs best in all naturalness metrics.

	Method	PSNR↑	SSIM↑	RESPONSE↑
	ORIGINAL	∞	1.0	100
	AMT-GAN	19.50	0.7873	33
MobileFace	DIM	28.23	0.7816	3
	TIP-IM	25.24	0.7567	1
	FRIA	**28.84**	**0.7941**	**63**

Table 6: Evaluation of Naturalness on ResNet50. Our FRIA performs best in all naturalness metrics.

	Method	PSNR↑	SSIM↑	RESPONSE↑
	ORIGINAL	∞	1.0	100
	AMT-GAN	19.50	0.7873	27
ResNet50	DIM	28.59	0.7875	20
	TIP-IM	25.14	0.7570	1
	FRIA	**28.82**	**0.7925**	**52**

In addition, in Fig. 6, we show the questionnaire we used to collect the response metrics, where we set two questions, each containing one original probe image and four encrypted images generated by AMT-GAN, DIM, TIP-IM, and our FRIA, respectively. To ensure fairness, we disordered the order of these images' placement.

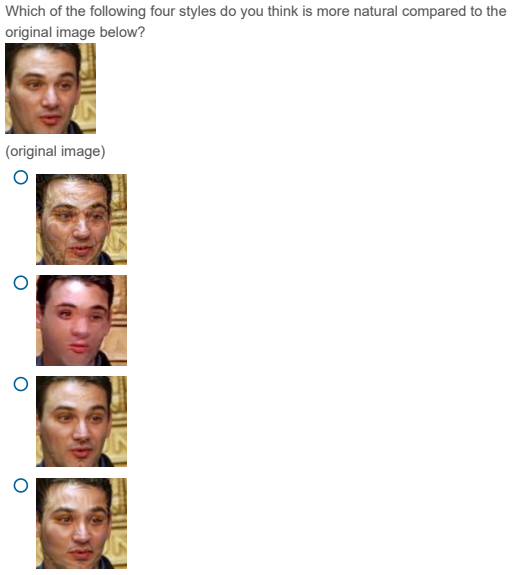

Figure 6: The presentation of one question in the questionnaire shows that one question contains four scrambled options corresponding to four different methods of encrypted face generation.

In Fig. 7, we have selected 20 original probe images and the corresponding encrypted faces generated using our FRIA to display, the left is the original probe image, and the right is the encrypted face generated by FRIA.

C ABLATION STUDIES

In this section, we will perform an ablation study of the components of FRIA. Specifically, we conduct several pairs of experiments and analyze them as follows:

(1) To demonstrate the effectiveness of selecting the average feature, we compare the performance of the average feature to that of the farthest feature, which is obtained by selecting a face image in the reference set D_{ref} whose feature is the farthest from the

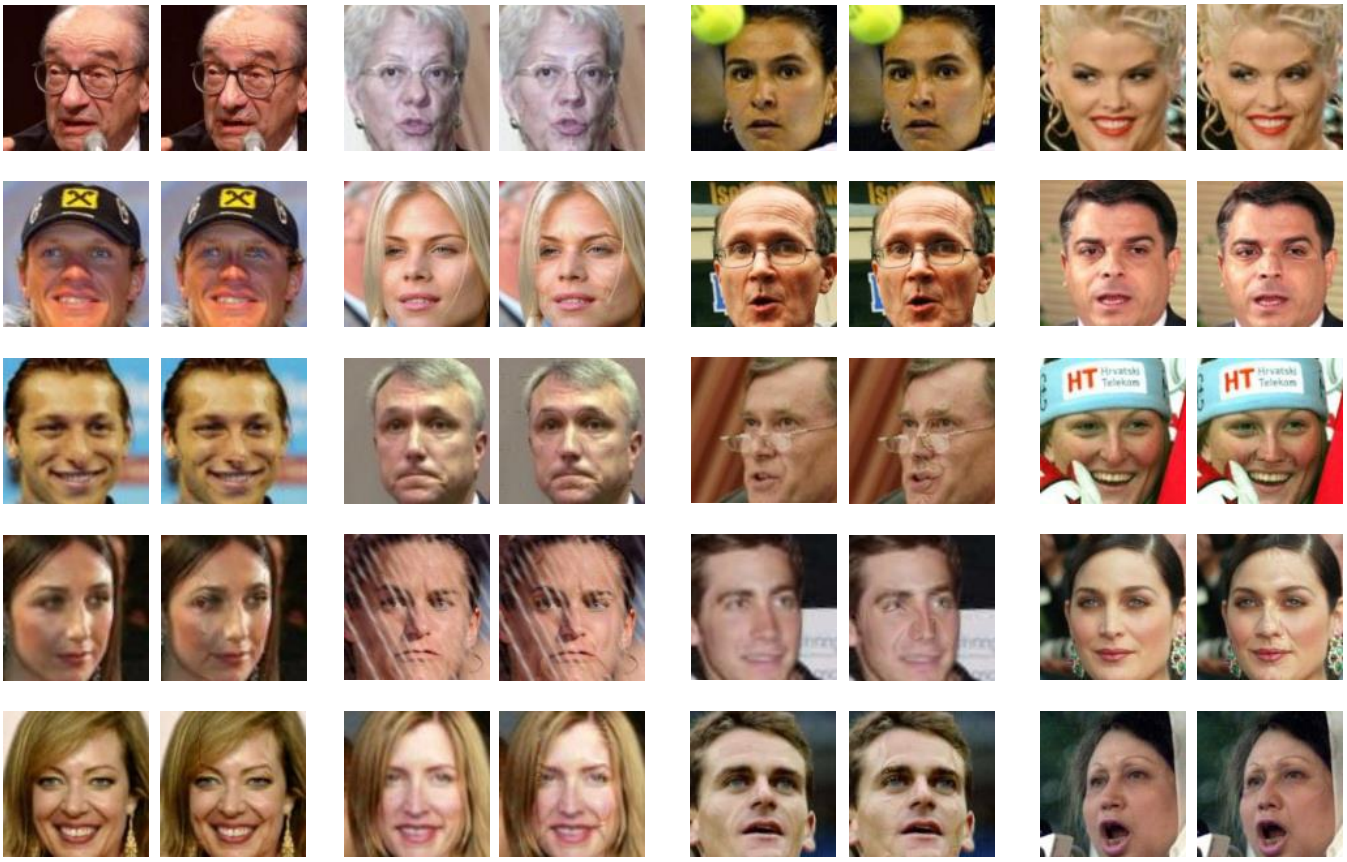

Figure 7: Evaluation of naturalness. The left is the original probe image, and the right is the corresponding encrypted face generated by FRIA.

Table 7: Performance comparison of farthest features and average features. The differences are marked.

	Method	ArcFace		MobileFace		ResNet50	
		ESR-1↑	ESR-5↑	ESR-1↑	ESR-5↑	ESR-1↑	ESR-5↑
ArcFace	FRIA-FARTHEST	100	100	96.4	93.0	91.8	80.6
	FRIA	**100(+0.0)**	**100(+0.0)**	**96.6(+0.2)**	**94.2(+1.2)**	**92.0(+0.2)**	**82.0(+1.4)**
MobileFace	FRIA-FARTHEST	69.6	58.8	100	100	94.2	88.6
	FRIA	**80.4(+10.8)**	**70.6(+11.8)**	**100(+0.0)**	**100(+0.0)**	**97.8(+3.6)**	**96.0(+7.4)**
ResNet50	FRIA-FARTHEST	71.6	55.0	96.8	91.8	100	100
	FRIA	**81.8(+10.2)**	**70.6(+15.6)**	**94.7(−2.1)**	**95.8(+4.0)**	**100(+0.0)**	**100(+0.0)**

feature of the probe image $\mathbf{x}^p$, known as FRIA-FARTHEST. We utilize ESR-1 and ESR-5 as evaluated matrices by choosing ArcFace as a substitute model to attack ArcFace, MobileFace, and ResNet50.

As shown in Tab. 7, using average features outperforms the most distant features, and the former performs better in ESR-5. This result implies that average features can bring a probe image closer to many identities. In contrast, the latter can only require it to be close to a single identity, and therefore the most distant features cannot guarantee transferability in a black-box attack.

(2) We select ArcFace as a substitute model to attack MobileFace to demonstrate the significance of incorporating an adaptive adjustment strategy (AAS) into FRIA, *i.e.,* to enhance the performance of the frequency restrict (FR).

Table 8: The effectiveness of adaptive adjustment strategy.

Method	ESR-1↑	ESR-5↑	PSNR↑	SSIM↑
FRIA w/o FR, AAS	**96.8**	**95.0**	28.16	0.7769
FRIA w/o AAS	**96.8**	**95.0**	28.17	0.7769
FRIA	96.6	94.2	**28.99**	**0.7931**

As shown in Tab. 8, the encrypted face's PSNR and SSIM did not improve by only adding the frequency restriction. However, after implementing the adaptive adjustment strategy, the PSNR and SSIM of the encrypted face improved by 0.82 and 0.0164, respectively. Adding an adaptive adjustment strategy may mitigate the conflict between identity-agnostic (IA) and frequency-restricted (FR).